Progress in Natural Science: Materials International 31 (2021) 180–191

HOSTED BY

Contents lists available at ScienceDirect

Progress in Natural Science: Materials International

journal homepage: www.elsevier.com/locate/pnsmi

Original Research

Direct ink writing of polycaprolactone / polyethylene oxide based 3D constructs

Bin Zhang [a], Se Hun Chung [a], Susan Barker [b], Duncan Craig [c], Roger J. Narayan [d], Jie Huang [a,*]

[a] Department of Mechanical Engineering, University College London, London, UK
[b] Medway School of Pharmacy, Universities of Greenwich and Kent, Kent, UK
[c] School of Pharmacy, University College London, London, UK
[d] Joint Department of Biomedical Engineering, University of North Carolina and North Carolina State University, Raleigh, NC, USA

ARTICLE INFO

Keywords:
Direct ink writing
Polycaprolactone
Polyethylene oxide
Ink rheology
Material characterisation
3D construct

ABSTRACT

There has been increasing interest over recent years in the application of three-dimensional (3D) printing technologies in the biomedical field. One such method is Direct Ink Writing (DIW); this approach has the potential advantage of allowing room-temperature deposition of materials, presented as an ink, to build complex architectures. DIW offers the ability to process biomaterials containing temperature-sensitive components. Due to the fabrication principles of DIW, there are specific rheological requirements that the ink must exhibit for the 3D construction. For this reason, hydrogel-based liquid feed stocks have been the focal point of ink development. As a consequence, studies based on inks comprising hydrophobic biomaterials, which are insoluble in water and hence unsuited to the hydrogel approach, have been limited.

In this study, we investigate novel inks that utilize polycaprolactone (PCL), a hydrophobic polymer, as the primary constituent by dissolving the polymer in solvent systems based on dichloromethane (DCM) and acetone (ACE). Moreover, polyethylene oxide (PEO) was incorporated into the PCL systems in order to extend the range of hydrophilicity of the systems. The rheological properties of the inks were investigated as a function of polymer composition and solvent system. Woodpile constructs of PCL and PCL/PEO were fabricated using DIW method and were assessed by a series of material characterisation. The type of solvent system had a noticeable impact on the ink rheology, which ultimately affected the surface properties. The incorporation of PEO particularly enhanced the roughness and wettability of the constructs. Our results support the use of DIW as a new means to process hydrophobic polymers for biomedical applications.

1. Introduction

3D printing (also referred to as additive manufacturing) is a technology that builds objects in a layer-by-layer fashion based on a predetermined digital model. This concept of manufacturing has attracted interest from the biomedical field as a new means of processing biomaterials into functional devices [1]. The utilisation of 3D printing allows the rapid construction of complex 3D geometries compared to conventional manufacturing techniques, which require moulding or lithographic masks [2]. In addition, the digital model in 3D printing is created either in a user-specified way or in compliance with medical imaging data to facilitate the fabrication of patient-specific structures [3]. This type of customisability from an architectural perspective has enabled 3D printing to be recognised as a platform for on-demand manufacturing.

A series of 3D printing technologies have been developed over the past decade that can be classified into two groups, namely light-based and extrusion-based approaches [1]. Although the former group provides higher printing resolution than the latter, the technologies (e.g., stereolithography and selective laser sintering) are limited to processing either photosensitive resins [4] or fine powders of thermoplastic polymers [5]. In contrast, extrusion-based platforms such as fused deposition modelling (FDM) and direct ink writing (DIW) may be applied to a greater range of processable materials [2] and thus have better versatility for biomedical applications than light-based approaches. FDM involves fusing thermoplastic filaments [6]. Polycaprolactone (PCL) is a US Food & Drug Administration-approved hydrophobic biomaterial that has been processed using the FDM method for implantable systems [7]. As an

* Corresponding author.
E-mail address: jie.huang@ucl.ac.uk (J. Huang).

https://doi.org/10.1016/j.pnsc.2020.10.001
Received 18 April 2020; Received in revised form 8 October 2020; Accepted 9 October 2020
Available online 21 October 2020

example of such biomedical applications, Reichert, Wullschleger *et al.* [8] used the FDM method to fabricate porous PCL-based scaffolds, which provided defect bridging for long bone repair. The results showed the formation of bone with high mechanical stability *in vivo* after twelve weeks. Zhou, Yao *et al.* [9] printed scaffolds containing PCL loaded with vancomycin; agar diffusion studies indicated sustained release and antibacterial activity against Staphylococci for more than four weeks. Indeed, hydrophobic biomaterials such as PCL have received widespread attention within the biomedical field as tissue grafts or scaffolds, due to their slow degradation rates allow for sustained structural integrity after implantation [8,10,11]. Such polymers also tend to be used for sustained release of agents such as anti-inflammatory agents or growth factors over weeks [9,12–14]. However, FDM requires the use of heat as the printing fidelity relies on solidification after the melt. This feature precludes the use of the platform for the incorporation of thermolabile additives such as cells, growth factors, or heat-sensitive drugs [15]. Given the requirement to incorporate heat-sensitive materials within scaffolds, the use of FDM in the field of tissue engineering may be subject to significant limitations.

Compared to FDM, DIW can operate in a heat-free environment as it involves extrusion of viscoelastic inks through a nozzle with the aid of a displacement-controlled driving mechanism [16]. The ink is technically in the form of a slurry or solution, depending on the component polymers, solvents, and additives. The ink used in the DIW process has to meet the following rheological requirements in order to print with high fidelity: (1) exhibit shear-thinning behaviour (reduction in viscosity with applied shear stress), (2) exhibit uniform flow of filament-like extrusion, and (3) demonstrate the ability to recover more than 80% of its viscosity after deposition [17–19]. These criteria have been identified from studies that utilised hydrogel-based inks [20,21]. Hydrogels are an attractive candidate for bioprinting in DIW since they possess similar properties to the natural extracellular matrix; in addition, the high water content allows the incorporation of cells. However, the applications of DIW for hydrophobic biomaterials such as PCL remains relatively limited. This is unfortunate as PCL is known for its propensity to form blends and composites that enable modulations of the physical properties of the scaffold [22–24]. For example, Remya *et al.* [25] blended hydrophobic PCL with a hydrophilic polymer, polyethylene oxide (PEO), and produced hybrid PCL/PEO fibres by electrospinning. The *in vitro* results showed that, in comparison to a PCL control, the group containing PEO degraded faster in phosphate buffered saline; it also exhibited enhanced cell attachment and proliferation as a result of improved surface wettability and enhanced surface micro-roughness. As PCL and PEO are immiscible, their contributions to the physicochemical properties of the composite may be readily and significantly tailored depending on the incorporation ratio [26]. This pair of polymers has not been processed via DIW to date; consequently, both PCL and hybrid PCL/PEO represent systems of interest in this study.

A limited number of studies have processed PCL only via DIW; these studies have utilised volatile solvents such as dichloromethane (DCM) or acetone (ACE) to dissolve the polymer [27,28]. Neither the rheological behaviour of the inks nor the effect of solvent choice has been extensively studied to date. Nevertheless, a number of studies have evaluated the effect of solvent volatility on the surface properties of polymeric products produced via other bio-fabrication platforms such as solvent casting and electrospinning/spraying [29–31]. It is well known that the surface properties of a polymeric matrix depend on both the type of solvent and the manufacturing process. Hence, a similar phenomenon may be expected to occur when polymer solutions are processed via DIW. To the best of the author's knowledge, the properties and their relationship to process parameters have not been investigated yet.

In this study, PCL and PCL/PEO inks were prepared based on a strategy of controlling solvent evaporation for processing 3D constructs. The polymer concentrations in the solutions were optimised using rheological measurements; ink flowing through the nozzle of the printer was evaluated numerically and experimentally. The chosen inks to fabricate 3D constructs were further investigated using a range of microscopic, diffraction, thermal, and wettability measurements. The aims of this study were to: (1) study the rheological properties of processable PCL and PCL/PEO inks, (2) investigate the influence of solvent and PEO incorporation on the surface properties of the printed constructs, and (3) evaluate the applicability of DIW as a tool for fabricating polymeric constructs.

2. Materials and methods

2.1. Materials

Polycaprolactone (PCL; average Mn ~ 80,000 and density, $\rho = 1.145$ g/cm^3) and polyethylene oxide (PEO; average Mn ~ 200,000 and $\rho = 1.210$ g/cm^3) were purchased from Sigma-Aldrich (UK). Dichloromethane (DCM; stabilised with 0.002% of 2-methyl-2-butene) and acetone (ACE) were obtained from VWR International Ltd (UK). The boiling temperature (T_b) and density (ρ) of DCM and ACE are 39.3 °C and 56.2 °C, and 1.325 g/cm^3 and 0.792 g/cm^3, respectively. All materials were used as received.

2.2. Ink formulation

2.2.1. Formulation procedure

After a preliminary screening of printability for a series of solvents, DCM and ACE were selected for the ink formulations. The polymer concentrations were narrowed down to 7.5% *w/w* and 15% *w/w* for the low (L) and high (H) end of the processable range. The PCL inks were prepared by dissolving PCL granules in DCM (D) or ACE (A) at 200 rpm under gentle magnetic stirring at 35 °C for 2 h. The DCM-based inks were coded as *L_D_PCL and H_D_PCL,* respectively; the ACE-based inks were named as *L_A_PCL*, and *H_A_PCL*, respectively.

PCL/PEO inks were formed by adding PEO to the PCL solutions under stirring conditions of 200 rpm at 35 °C for 3 h; distilled water (10% *v/v*) was added to the ACE. For filament formation during extrusion, the formulated inks must be neither too free-flowing nor too viscous. Therefore, only the 1:1 wt ratio of PCL:PEO was chosen for further study. The PCL/PEO inks were designated as *L_D_PCL/PEO and H_D_PCL/PEO* for DCM solvent-based systems; *L_A_PCL/PEO* and *H_A_PCL/PEO* refer to the ACE solvent-based systems, respectively.

2.2.2. Ink characterisation

In the manual dispensing test, as shown in Fig. 1 (a), for each ink sample, a 24 G nozzle tip of 20 mm length was attached to the end of the 3 mL syringe. The pressure was manually placed on the plunger until the material was extruded; the images were captured by the camera (Canon EOS M50, Canon, Melville, LA, USA).

The rheological properties of the formulated inks were measured using the MCR301 rheometer (Anton Paar, Ostfildern, Germany) with a 25 mm plate-plate (0.5 mm distance) and a solvent trap to minimise solvent evaporation. All of the measurements were performed at 25 °C and conducted in triplicate using approximately 0.5 mL of ink. Continuous flow ramps were conducted by varying the shear rate logarithmically from 0.01 to 100 s^{-1}. To determine the linear viscoelastic region, an oscillatory stress sweep test was performed over the strain range (from 0.01 to 100%). To evaluate the yield stress of the tested samples at a constant frequency of 1 Hz, the stress applied increased from 0.1 Pa until the material yielded.

To simulate 3D printing conditions, a creep recovery test was carried out using three intervals. In the rest interval, a low shear rate (1 s^{-1}) was applied for 10 s. Then, a constant high rate (200 s^{-1}) was applied for 1 s. The recovery interval was carried out with a shear rate of 1 s^{-1} for 90 s. The viscosity recovery percentage at the 90 s was calculated by comparing the viscosity to the initial viscosity at the rest interval (10 s).

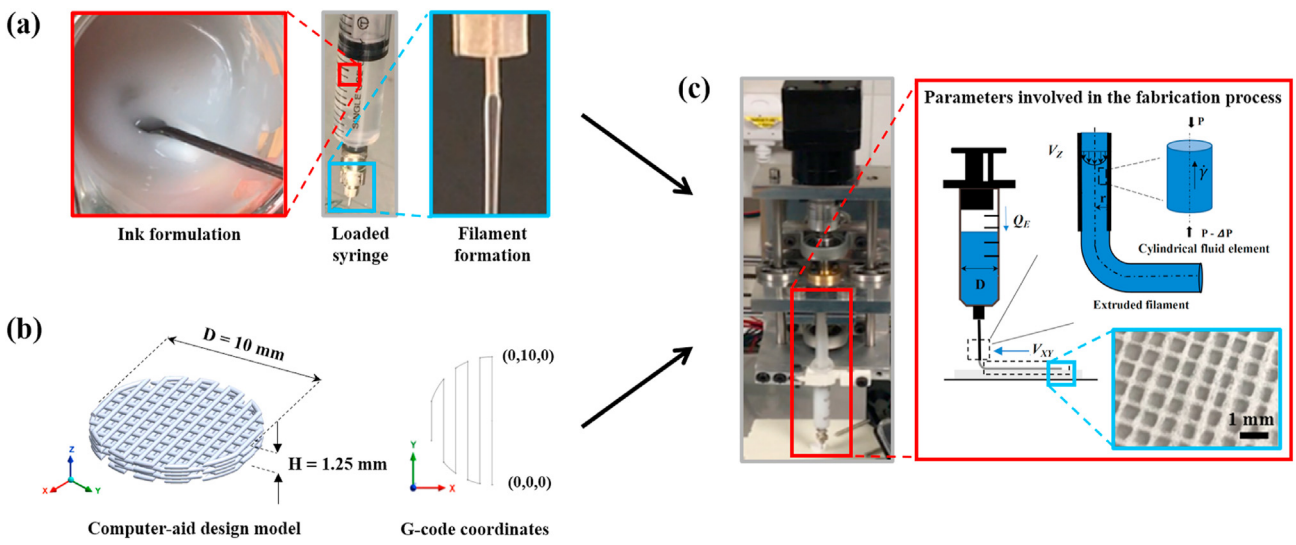

Fig. 1. Desktop DIW printer and flow chart of the fabrication process; (a) material preparation system - inks were formulated to investigate the manual dispensing and ink rheological behaviour; (b) data processing system-suitable G-code was developed based on the predesigned CAD model; (c) computer control system-the construct was printed after the investigations of the printing process parameters, including the extruded fluid rate Q_E and printing speed on the XY plane V_{xy}.

2.3. 3D construct fabrication

2.3.1. Structural designs

A five-layer woodpile construct was designed using computer-aided design (CAD) software (SolidWorks 2005, Dassault Systèmes SolidWorks), as shown in Fig. 1 (b). The height of the layer was 0.25 mm, each layer comprising parallel filaments with the width of 311 μm, which is equivalent to the 24 G nozzle diameter. The subsequent layers were stacked at 90° in the transverse plane to the prior level. G-codes of the designs were generated using MATLAB in accordance with the CAD models, which gave instructions to the printer and controlled the relative positions of the work stage and nozzles in the *X, Y,* and *Z* direction as well as the extrusion rates.

2.3.2. Mathematical model

The DIW operation parameters were studied, as shown in Fig. 1 (c), including the printing speed on the XY plane (V_{xy}) and ink velocity on Z-axis (V_Z), and the extruded fluid rate (Q_E). According to the power law fluid model, the velocity profile along a nozzle tube on the Z-axis is given by Equation (1) [32].

$$V_Z = \left(\frac{d}{2}\right)^{1+\frac{1}{n}} \left(\frac{\Delta P}{2mh}\right)^{\frac{1}{n}} \left(\frac{n}{n+1}\right) \left[1 - \left(\frac{2r}{d}\right)^{1+\frac{1}{n}}\right] \tag{1}$$

where ΔP is the extrusion pressure-the pressure difference between the inlet and outlet of the nozzle tip, r is the radial coordinate, and d and h are the nozzle tip diameter and printed length, respectively. The extrusion flow rate Q_E and the generated shear rate ($\dot{\gamma}$) are defined by Equation (2) [32] and Equation (3) [33].

$$Q_E = \left(\frac{\Delta P d}{4mh}\right)^{\frac{1}{n}} \left[\frac{n\pi d^3}{8(3n+1)}\right] \tag{2}$$

$$\frac{dV_Z}{dr}\Big|_{\frac{d}{2}} = \dot{\gamma} = \frac{32Q_E}{\pi d^3}\left(\frac{3}{4} + \frac{1}{4n}\right) \tag{3}$$

The nozzle tip diameter influences the shear rate. When the extrusion flow rate Q_E is fixed, small nozzle tip diameter requires a higher pressure to dispense the material. If the nozzle diameter d is fixed, the wall shear rate increases with the extrusion flow rate. In this study, the extrusion flow rates were set to resemble the DIW printing process, and the relationship between the solvent selection and the DIW printing parameters were investigated.

$$E = \frac{4Q_E L}{V_{xy}\,\pi\, D^2} \tag{4}$$

Equation (4) shows the relationship of the downward movement distance of the piston during the printing (E) with the extrusion flow rate Q_E, and printing speed V_{xy}. D is the inner diameter of the syringe that is used to extrude inks, and L is the printed filament length. The value of E was set within the G-code for DIW printing, depending on the preset extrusion rate Q_E, and printing speed V_{xy}.

2.3.3. Desktop DIW printing process

The desktop DIW printer used in this study was modified from a commercial Prusa i3 fused deposition modelling (FDM) printer. The filament print head was replaced with a customised syringe-based extruder. Fig. 1 (c) describes the processes involved in DIW technology. The motion system comprises a print bed and a nozzle. The print bed moves in the Y direction, and the nozzle moves in X and Z directions. Linear actuator stepping motors drive the motion in the Z direction and control the piston with an overall resolution of 0.001 mm/step and a 1.8° step angle. A 3 mL syringe was used for the extrusion, and the extruded volume resolution was 6×10^{-5} mL/step.

A continuous and consistent extrusion of polymer inks is of great importance during the DIW printing process. The filament extrusion can be affected by the ink rheological behaviour and printing parameters (i.e., printing speed V_{xy} and extrusion rate Q_E). To optimise the DIW printing parameters, the flow rate Q_E of 0.48–1.44 mm^3/s and printing speed V_{xy} in the range from 2.5 to 12.5 mm/s were set using Pronterface software (https://pronterface.com). A glass slide was used as a collecting substrate for printing, and the print samples were easily taken off from the substrate after drying.

2.3.4. DIW printed pattern and surface morphology

A stereomicroscope (SM-3TZZ-54S-10 M; AmScope) was used to observe the DIW printed patterns. The width of printed filament was quantified by measuring at least 50 filaments in Image J software (http://rsb.info.nih.gov/ij/); the data was exported for analysis, and the statistical distributions were plotted using Origin software (Origin Lab, USA). The results were presented as the mean ± standard deviation. An index of relative filament deviation ($\sigma_{filament}$) was proposed to evaluate

the filament width of DIW printed constructs, it was defined in Equation (5).

$$\sigma_{filament} = \frac{W_{filament}}{d} - 1 \quad (5)$$

where $W_{filament}$ is the printed filament width and d is the nozzle diameter used. The index of relative filament deviation $\sigma_{filament}$ as a function of the choice of printing parameters was calculated and compared as an assessment of the shape fidelity of printed filaments.

The surface morphology of the printed samples was observed using a S–3200 N (Hitachi, Japan) scanning electron microscope (SEM). The samples were first sputter-coated with a thin layer of gold (10 nm), and the images were obtained at an acceleration voltage of 5 kV from low to high magnifications (× 500–10k).The surface roughness of the samples was quantified using a profilometer (Keyence VHX 2000, Osaka, Japan). The roughness was measured over an area of 600 μm (length) x 60 μm (width) on the three different filaments on the sample surface. The surface roughness in terms of an arithmetic average (Ra) was obtained as a function of the printing conditions.

2.3.5. Physicochemical characterisation

The phases structure of the DIW printed constructs were investigated using a D5005 X-ray diffractometer (XRD, Siemens, Germany) with a monochromatic CuKα radiation (wavelength = 1.54056 Å). Scanning was performed on the printed samples from 5° to 35° 2θ at a step size of 0.02° and a scan rate of 0.02°/min. The chemical bonding states and atomic concentrations in the printed samples were examined by X-ray Photoelectron Spectroscopy (XPS; Phoibos 150 analyser, SPECS GmbH, Germany) to compare the electron binding energy intervals. The peak position and atomic concentration of elements (At%) were obtained, and the ratio of oxygen and carbon (O/C) was calculated for quantitative comparison. Each sample was analysed in duplicate; the average was compared.

2.3.6. Thermal analysis

The thermal properties of raw polymers and printed PCL/PEO samples were characterised using a Hi-Res 2950 thermogravimetric analysis (TGA) and a Q1000 differential scanning calorimetry (DSC), respectively, (both from TA Instruments, USA). The tests were conducted after leaving the samples at ambient temperature for 12 h post-printing. All measurements were obtained in duplicates and TA Universal Analysis 2000 was performed for the data analysis.

For TGA, printed samples (~5–10 mg) were placed in open aluminum pans (PerkinElmer, UK), and were heated from 30 °C to 400 °C with a ramp of 10 °C/min; they were subsequently purged under a flux of nitrogen gas. The percentage of weight losses and onset thermal degradation temperatures (T_d) were recorded from the TGA traces obtained.

DSC was performed to acquire the peak melting temperatures (T_m) of the raw polymers and printed samples. The samples (~5–15 mg) were individually placed in an aluminum DSC pan (PerkinElmer, UK), and sealed using a lid with a pin-hole punched through. All samples were equilibrated at 0 °C and then heated at a rate of 2 °C/min to the desired temperatures. Nitrogen purge gas with a flow rate of 50 mL/min was used throughout the experiments.

2.3.7. Wettability

Contact angle measurements were performed to evaluate the wettability of the DIW printed surface. A sessile drop method was used to measure the contact angle by depositing ultrapure water (4×10^{-4} μL) on the surfaces of the printed filament using an optical contact angle meter (OCA 15 EC; Dataphysics Instruments GmbH, Germany). All of the measurements were performed at 21 °C, and the gradual change of water contact angle was captured with a digital camera at three different places on each sample.

All of the quantitative data were expressed as the average ± standard error of the mean. The numerical data were analysed via Student's *t*-test to determine the differences among the groups. Statistical significance was indicated by (*), which represents a p-value < 0.05; (**), which represents a p-value < 0.01; and (***), which represents a p-value < 0.001. If the p-value > 0.05, no difference was noted.

3. Results

3.1. Ink printability assessment

A two-step assessment was proposed to characterise the material properties associated with printability in order to further understand the design factors that facilitate DIW fabrication [19,34]. The first assessment step, manual dispensing, is an initial screening method that focuses on the ability of the inks to form filaments rather than droplets such that the formed filaments stack in a layer-by-layer manner to obtain the 3D constructs. The second step requires rheological measurements to identify the properties of the inks before, during, and after extrusion in the printing process. Thus, we utilised (a) a shear viscosity test to understand the shear-thinning properties of the material, (b) a shear stress amplitude ramp assessment to obtain the ink linear viscosity region and yield stress, and (c) a recovery test to observe the ink recovery behaviour after being exposed to high shear rates by applying an alteration of high and low shear rates. To understand the influence of various parameters such as the polymer concentration, solvent type, and incorporation of PEO, on the ink printability, the two-step printability assessments were performed on all of the ink formulations.

3.1.1. Manual dispensing

The formation of a consistent and cylindrical filament by manual extrusion is a rapid and highly effective way to assess the preliminary printability of an ink. To simulate the DIW printing process, the inner diameter of a nozzle (311 μm) was selected to match the extrusion system used for DIW printing. The dispersing behaviour of PCL and PCL/PEO solutions with low and high concentrations is shown in Fig. 2. The inks *L_D_PCL, L_A_PCL* and *L_D_PCL/PEO* formed droplets while the inks *H_D_PCL,H_A_PCL, H_D_PCL/PEO, L_A_PCL/PEO,* and *H_A_PCL/PEO* were able to form filaments. This result suggests that the concentration of the polymer is critical for filament formation, as the majority of the inks with lower concentrations were unsuccessful. Those inks that formed filaments passed the first-step printability assessment for extrusion-based printing. Although increasing the polymer concentration can improve the filament formation, the ink viscosity cannot be too high, as it would not be extruded out from a syringe; in addition, the needle will be forced out if higher pressure is applied.

3.1.2. Ink rheology

Rheological properties of the formulated inks were characterised from shear rate-dependent viscosity, yield stress, and recovery behaviour after applying a high shear rate. The consistency index (m) and the power law index (n) were calculated by applying the power law model to the shear rate-viscosity profiles, so the degree of shear-thinning could be ascertained. The yield stress was determined via shear stress ramps and predicting the extrusion behaviour at DIW printing induced shear rates. Finally, the recovery of the inks after exposure to shear rates similar to those during DIW printing was evaluated.

Firstly, the viscosity of the formulated PCL and PCL/PEO based inks was evaluated through steady-state shear viscosity measurements. Fig. 3 (a, b) shows the viscosity curves with the shear rate for the PCL and PCL/PEO inks with different concentrations in ACE and DCM solvents.

The viscosity curves were fitted using the power law model [32], which is given by Equation (6).

$$\eta(\gamma) = m\gamma^{n-1} \quad (6)$$

where m is the consistency index, which is associated with the magnitude

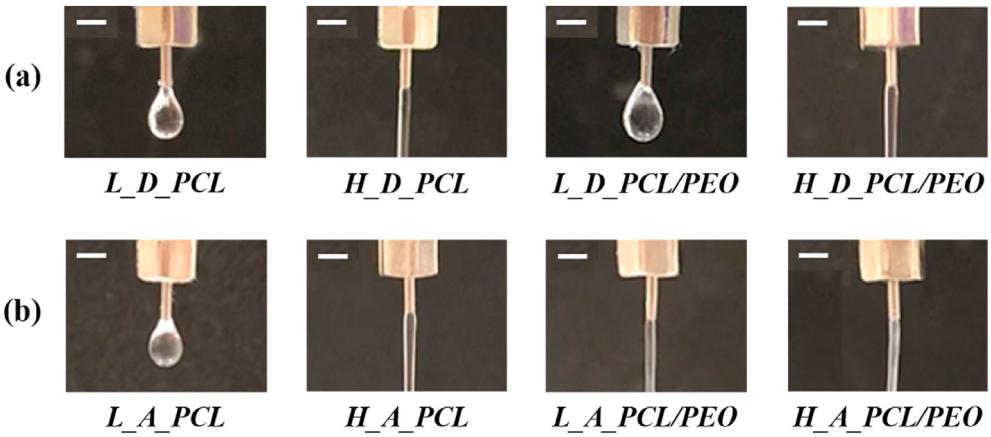

Fig. 2. Printability assessment with manual dispensing of PCL (a) and PCL/PEO (b) based inks with low and high concentrations. The scale bar represents 1 mm.

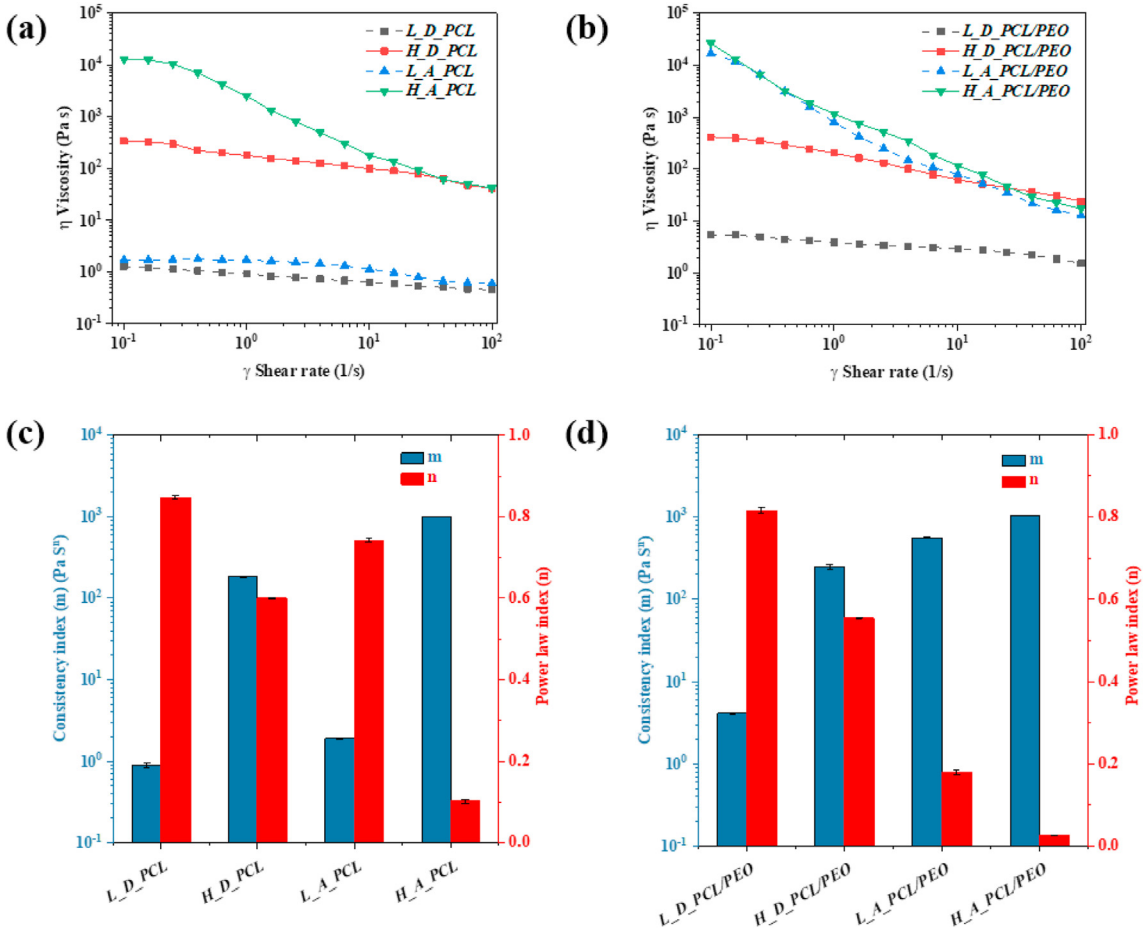

Fig. 3. Viscosity flow curves of PCL (a) and PCL/PEO (b) based inks in DCM and ACE solvents with low and high concentrations; the consistency index m and power law index n of PCL (c) and PCL/PEO (d) based inks, obtained from the power law model fitting.

of the viscosity. The term n is the power law index, defines the viscosity behaviour: (i) shear-thickening if $n > 1$, (ii) Newtonian if $n = 1$ or (iii) shear-thinning if $n < 1$. The curve of $\ln \eta$-$\ln \gamma$ was plotted based on the ink viscosity curves. By fitting the slope and intercept, the consistency index m and the power law index n of the inks were obtained, respectively. Fig. 3 (c, d) summarises n and m results of PCL and PCL/PEO based inks, and their correlation coefficients (R) were greater than 0.99. The n values of all inks are less than 1, which indicates that all inks are non-Newtonian fluids with shear-thinning behaviour. The larger the deviation of n from 1, the more non-Newtonian is the behaviour of the fluid [35]. All the inks tested are suitable for extrusion-based printing: they pose a high viscosity at the low shear rate and a low viscosity at a high shear rate.

Upon increasing the polymer concentrations from 7.5 to 15%*w/w* for both PCL and PCL/PEO based inks, the power law index n decreased, while the consistency coefficient m increases, which indicated more prevalent shear-thinning behaviour. The viscosity for the lower concentration of PCL based inks exhibits shear-thinning behaviour after a Newtonian plateau. The power law index n further decreased with the

addition of PEO: from 0.60 to 0.55 for the DCM-based ink and from 0.10 to 0.03 for the ACE-based system. The drop in viscosity with shear stress of PCL/PEO inks is greater for the ACE-based inks.

Secondly, an oscillatory stress sweep test was performed on the inks that were able to extrude filaments by manual dispensing so as to evaluate the viscoelastic behaviour of these inks. The yield stress was determined using the intersection point of two tangents, one in the linear viscoelastic region in which the inks were deformed elastically, and another in the region in which the storage modulus values dropped. When the ink is at rest, the interacting forces among polymer chains form a stable, three-dimensional network, and the material acts rheologically as a condensed solid-state system. After exceeding the yield stress point, the ink polymer superstructure breaks down, and the material starts to flow.

Both DCM and ACE based PCL inks (*H_D_PCL* and *H_A_PCL*) were prone to flowing away at the shear stress ramp at 0.1 Pa; hence, the yield stress could not be accurately determined. However, those inks with added PEO were able to provide data for the oscillatory stress sweep test when the applied shear stress increased from 0.1 Pa until the yield points were obtained. This result may indicate that the addition of PEO improves the solid-like behaviour of the inks. The yield stress results indicated that the polymer concentration is of clear importance; the low PCL/PEO in ACE ink (*L_A_PCL/PEO*) started to yield when the shear stress was 43.0 Pa, while the yield stress increased with the high polymer concentration; the *H_A_PCL/PEO* ink was approximately eight times higher (347.7 Pa). It was also observed that the choice of solvent had an influence on the yield stress. The yield stress (765.2 Pa) of the DCM-based ink (*H_D_PCL/PEO*) was more than two times higher than the ACE-based ink at the same concentration.

Thirdly, the ability of the inks to recover was examined by the creep recovery test. The results show that the viscosity of all of the inks were able to return to original values with time. This test corresponds to the DIW printing process in that the ink flow through the nozzle tip under shear; thereafter, the viscosity decreases as a function of time to a constant value. For the DCM-based PCL/PEO ink (*H_D_PCL/PEO*), the initial recovery was nearly 93% after the high shear rate removal and became full recovery at circa 100 s; however, ACE based PCL/PEO inks (*L_A_PCL/PEO* and *H_A_PCL/PEO*) were not able to recover fully at 100 s, although the recovery percentage was higher (81%) for the high concentration ink (*H_A_PCL/PEO*) in comparison to that of the low one (44% for *L_A_PCL/PEO*). As the initial viscosity recovery of an ink must be higher than 80% to enable 3D printing [36], *L_A_PCL/PEO* ink was deemed to be not suitable for the DIW process, even though it was able to form a filament. Therefore, only high concentration PCL/PEO inks (*H_D_PCL/PEO* and *H_A_PCL/PEO*), with viscosity recovery percentages higher than 80%, were selected for further investigation of the influence of solvents on the DIW printing process.

3.2. Mathematical analysis of ink flow within a printing nozzle

Using the theoretical extrusion pressure, velocity and shear rate, the theoretical extrusion behaviour of materials inside a printing nozzle could be obtained. It is possible to predict spatial distributions of the parameters inside the nozzle for both DCM and ACE based PCL/PEO inks (*H_D_PCL/PEO* and *H_A_PCL/PEO*). Besides the parameters dictated by the DIW printer setup for dispensing, such as needle radius, needle length, and extrusion rate, the power law index n and the consistency index m obtained from the shear viscosity measurements also play essential roles.

The profiles of velocity on the Z-axis (V_Z) of DCM and ACE based PCL/PEO (*H_D_PCL/PEO* and *H_A_PCL/PEO*) inks along a radial axis of 155.5 μm nozzle are shown in Fig. 4 (a, b), and the parameters were calculated from Equation (1). For both inks, with the increasing extrusion fluid rate from 0.48 to 1.44 mm^3/s, the extrusion pressure (ΔP) and induced wall shear rate ($\dot{\gamma}$) were raised; however, the velocity (V_Z) profile along the nozzle tube decreased towards the needle wall. This is similar to the

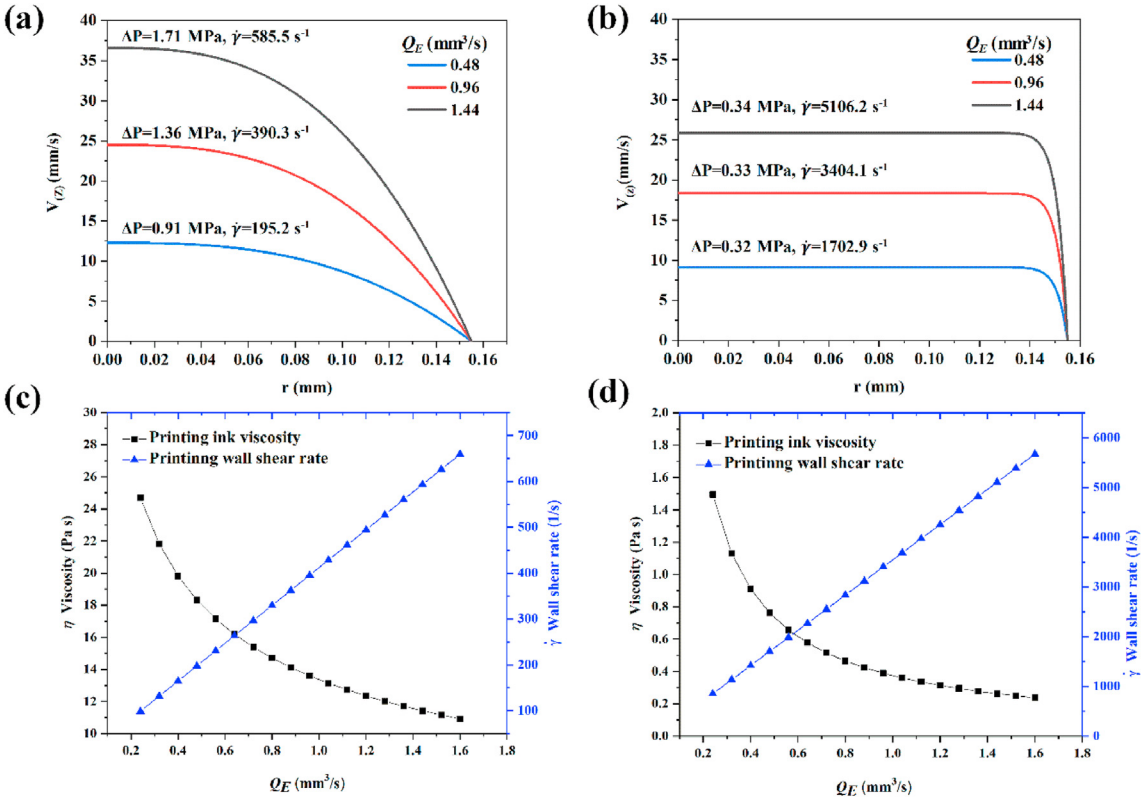

Fig. 4. The ink velocity (Z-axis) (V_Z) profile inside nozzle tip for *H_D_PCL/PEO* (a) and *H_A_PCL/PEO* (b) during the DIW extrusion condition; printing viscosity (η) and wall shear rate ($\dot{\gamma}$) as a function of the extrusion fluid rate (Q_E) for *H_D_PCL/PEO* (c) and *H_A_PCL/PEO* (d).

parabolic profile within a pipe of a fully developed fluid; friction is also important in the flows since internal friction resists motion. A fluid with high viscosity has a large amount of internal friction; when a fluid is in contact with a static solid surface (nozzle wall), adhesion can slow the flow of the fluid [37,38]. The results show that the velocity profile of DCM ink gradually decreased from the middle of the needle tip to the wall of the needle tip; on the other hand, the velocity (V_Z) of the ACE ink kept a similar level within the needle and changed suddenly near the nozzle wall. This result could be associated with the strong shear-thinning behaviour of the ACE ink, which maintains higher viscosity under a low shear rate than the DCM ink.

Fig. 4 (c, d) show that the shear rate of both inks experienced linearly increases as a function of the extrusion flow rate (Q_E). Those profiles were calculated from Equations (2)–(4). The ink shear-thinning behaviour under conditions of extrusion could be beneficial in allowing the viscosity to decrease at the time of processing, thereby allowing the ink to flow out and deposit. However, when under the same extrusion rate (i.e., 0.48 mm^3/s), the ACE ink (*H_A_PCL/PEO*) exhibited approximately a nine times higher shear rate (1702.9 s^{-1}) than the DCM ink (195.2 s^{-1} for *H_D_PCL/PEO*) as predicted from mathematical modelling (Fig. 4 (c, d)). The higher shear rate for the ACE based ink, as well as the lower initial recovery percentage and slower recovery rate after removing from a high shear rate (i.e., 200 s^{-1}) in the creep recovery test, could explain why the ACE ink may be prone to printing failure while the DCM-based ink (*H_D_PCL/PEO*) could be more suitable for successful extrusion.

3.3. Shape fidelity analysis

3.3.1. Effect of operational parameters

The printing parameters such as the extrusion rate (Q_E) and printing speed in the *XY* plane (V_{xy}) directly influence the ink deposition. At a fixed the extrusion rate (i.e., 0.48 mm^3/s), the width of printed filament varied depending on the printing speed, as shown in Fig. 5 (a) for the DCM based ink (*D_PCL/PEO*). When the print speed was 2.5 mm/s, the printed filament width was 400 ± 10.0 μm, which was higher than the nozzle diameter (311 μm). When the printing speed increased to 7.5 mm/s, the printed filament was stretched, and the width of the deposited filament was reduced to 241 ± 12.9 μm, which was lower than the nozzle diameter. Once the velocity increased to 10 mm/s, the deposition was interrupted, and the filaments no longer exhibited a consistent and uniform diameter.

Similar trend was observed for the ACE-based ink (*A_PCL/PEO*), the comparison of the DIW printed filament width of both inks under various extrusion fluid rates (0.48–1.44 mm^3/s) and printing speeds (2.5–12.5

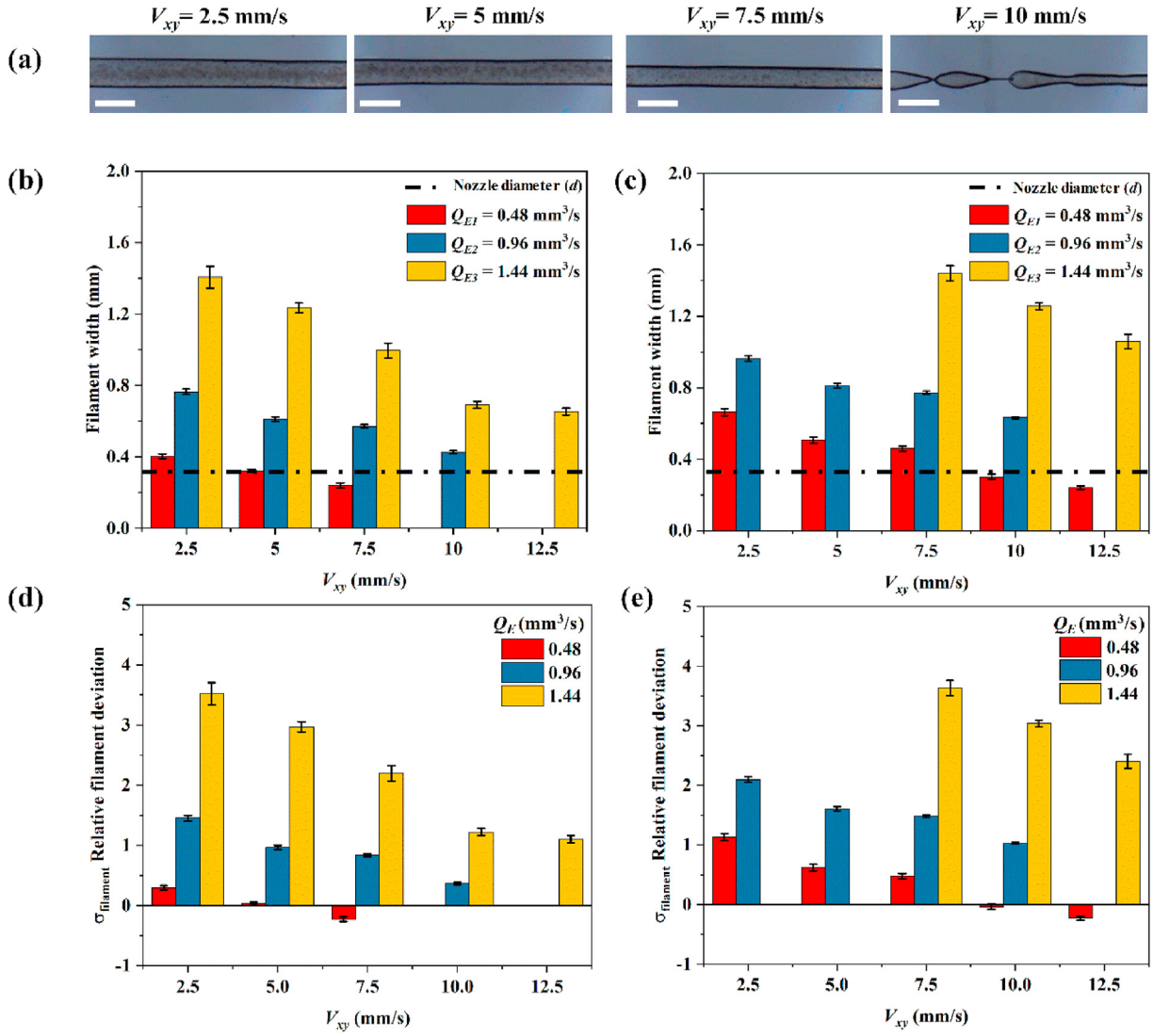

Fig. 5. Printed filament width of *D_PCL/PEO* changes with various print speed V_{xy} when the extrusion rate Q_E = 0.48 mm^3/s, the scale bar is 500 μm (a); the DIW printed filament width of *D_PCL/PEO* (b) and *A_PCL/PEO* (c) and the relative filament deviation ($\sigma_{filament}$) of *D_PCL/PEO* (d) and *A_PCL/PEO* (e) under the designated printing speed and extrusion rate.

mm/s) is shown in Fig. 5 (b, c). The width of DIW printed filaments decreased with an increase in print velocity (V_{xy}) or a reduction in extrusion fluid rate (Q_E), and vice versa.

The index of relative filament deviation ($\sigma_{filament}$), calculated from Equation (5), was used to evaluate the DIW printed filaments, it approaches 0 when the filament width ($W_{filament}$) matches the nozzle diameter (d). The deviation indexes at various printing parameters are compared in Fig. 5 (d, e), the relative filament deviation is closest to 0 at the printing speed V_{xy} of 5 mm/s and the extrusion fluid rate Q_E of 0.48 mm^3/s for the DCM based ink. These operation parameters were used for building 3D constructs subsequently in terms of a better shape fidelity by matching of the nozzle diameter. Similarly, the printing speed V_{xy} of 10 mm/s and the extrusion fluid rate Q_E of 0.48 mm^3/s are considered as the best set up for the ACE-based ink.

3.3.2. 3D constructs

The 3D constructs of PCL and PCL/PEO blend were built in a layer-by-layer manner using DIW from both DCM and ACE based inks. The optical micrographs of printed samples (five layers) are shown in Fig. 6 (a). The width of printed filaments was measured and compared with the applied nozzle diameter, as shown in Fig. 6 (b). The relative filament deviation indexes ($\sigma_{filament}$) were 0.45 ± 0.08, −0.27 ± 0.08, 0.04 ± 0.01, and −0.19 ± 0.09 for the DIW-printed samples *D_PCL*, *A_PCL*, *D_PCL/PEO*, and *A_PCL/PEO*, respectively (Fig. 6 c). The deviation index from *D_PCL/PEO* is closest to 0 when compared to others, it showed that the incorporation of PEO in PCL improved the stability of filament shape after extrusion, and the size was closest to the nozzle diameter. In general, the filaments printed form DCM-based PCL/PEO inks are more uniform than those of the ACE-based inks; this could be resulted from the higher (9 times) shear rate for the ACE-based ink than the DCM system, as simulated from the mathematical modelling (Fig. 4 c and d). This result combined with the lower ink recovery rate of the ACE ink may be associated with the inherent variability of the extrusion printing process reported by other researchers [39,40].

3.4. Thermal characterisation

TGA was performed to investigate whether any residual solvents remained in the printed parts after 12 h post-printing. Considering the boiling temperatures of DCM (39.3 °C) and ACE (56.2 °C), it is evident that all the solvents evaporated within 12 h since no weight loss was observed below 70 °C (Fig. 7(a)). The onset T_d value of raw PEO and PCL was 248.3 °C and 340.5 °C, respectively. Two onset T_d values (259.2 °C and 374.6 °C) were found in *D_PCL/PEO*, while 244.4 °C and 378.7 °C were in *A_PCL/PEO* samples; the lower T_d represents PEO while the higher corresponds to PCL. The T_d values of the printed samples corresponding to PEO were less than ±5% difference while the onset points representing PCL were visibly higher by 10%. Such shifts in onset temperature suggest that the thermal stability of PCL improves when blended with PEO.

The resultant thermal DSC traces of the raw polymers and PCL/PEO printed parts are shown in Fig. 7 (b). The observed melting peak (T_m) of raw PCL and PEO was 60.9 °C and 70.2 °C, respectively. The PCL/PEO blends have shown two distinct peaks clearly; 61.8 °C and 67.1 °C for *D_PCL/PEO* and 63.9 °C and 68.2 °C for *A_PCL/PEO*. The closely matching melting peaks of PCL and PEO with the corresponding peaks in the blended parts confirm that the two polymers showed poor miscibility in the matrix.

3.5. Material characterisation

X-ray diffraction (XRD) was used to determine the phase structure of

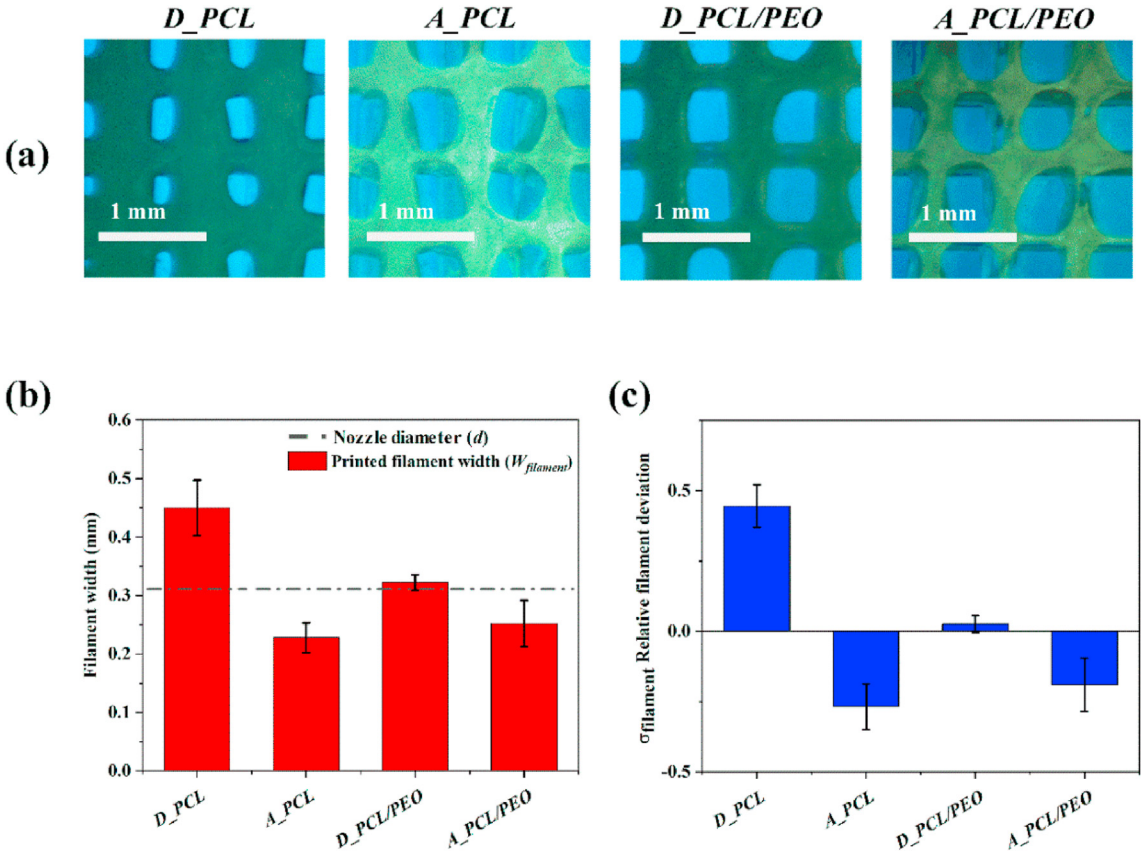

Fig. 6. Microscopy image (a), measurement of filament width (b) and relative filament deviation ($\sigma_{filament}$) (c) of DIW printed 3D constructs - *D_PCL*, *A_PCL*, *D_PCL/PEO*, and *A_PCL/PEO*.

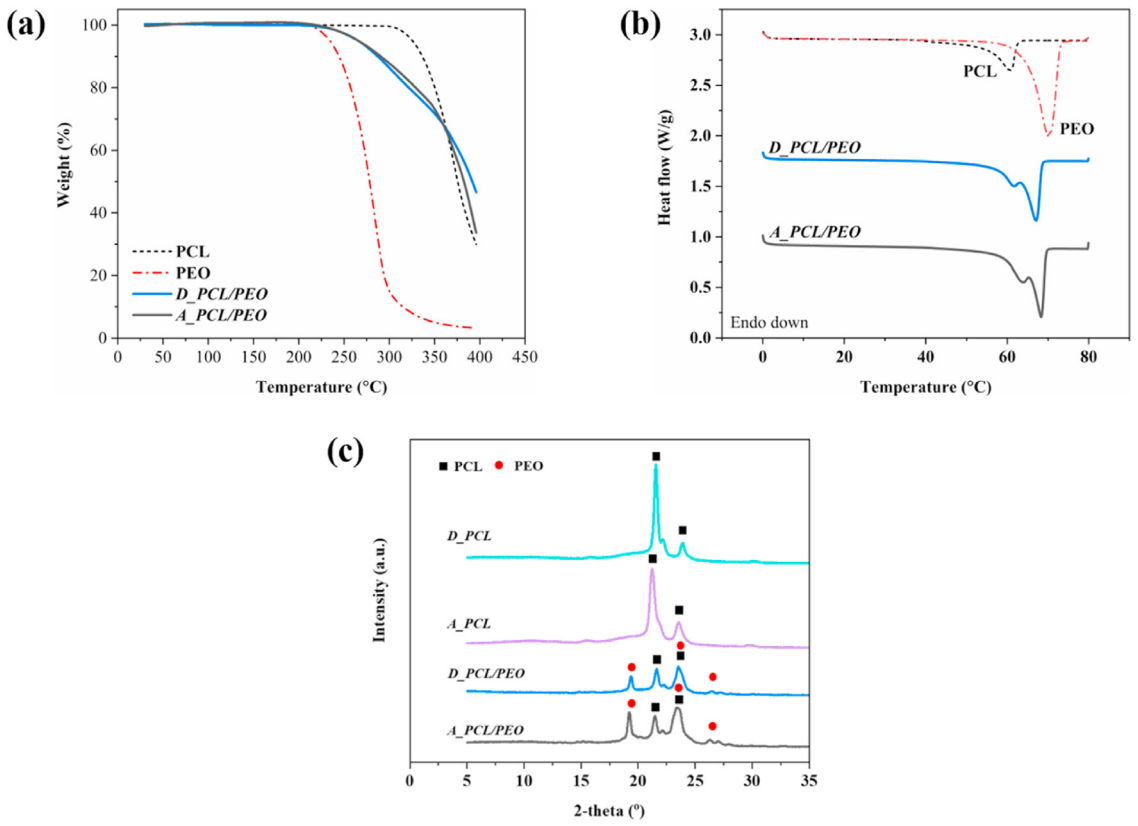

Fig. 7. Thermogravimetric analysis (a) and differential scanning calorimetry traces (b) of the raw polymers and printed PCL/PEO samples; XRD patterns (c) of printed samples - *D_PCL, A_PCL, D_PCL/PEO,* and *A_PCL/PEO.*

the biopolymer blends. If two polymers are immiscible, each crystal structure remains in the blends. XRD patterns of printed *D_PCL/PEO* and *A_PCL/PEO* are depicted in Fig. 7 (c). The peaks at angles 2θ of 21.4° and 23.8° correspond to the (110) and (200) crystallographic planes of the semi-crystalline nature of the PCL biopolymer [41], respectively. The pure PEO exhibits two characteristic peaks at angles around 2θ of 23° and 19° [42]. The decrease in intensity of the PCL peaks is associated with the addition of PEO. The characteristic of peaks of pure PCL were unchanged in both blends, suggesting that the incorporation of PEO did not significantly affect the crystalline structure of PCL.

X-ray photoelectron spectroscopy (XPS) was used to verify the surface elemental composition of the printed samples. Two separated peaks corresponding to C1s (284 eV) and O1s (532 eV) were seen in all of the XPS spectra. For a better understanding of the oxygen groups on the sample surface, the C1s and O1s peaks were further analysed. Three C bonding states at 285.2 eV, 286.5 eV, and 288.6 eV correspond to C–H, C–O, and O–C═O, respectively. The presence of PEO in the sample affected the binding energy and broadening the C 1s peaks. The oxygen-containing functional group is vital to surface properties such as hydrophilicity and hydrophobicity [43]. Table 1 summarised the carbon and oxygen atomic percentage for the *D_PCL*, *A_PCL*, *D_PCL/PEO* and *A_PCL/PEO* samples. With the addition of PEO, the O/C ratio of printed samples increased from 34.7% to 45.2% for the ACE-based ink, and from 36.1% to 50.2% for the DCM-based ink. Wettability is positively related to the surface oxygen content, with increasing of the O/C ratio, the surface becomes more hydrophilic.

Table 1
XPS survey data for the atomic component for the printed samples - *D_PCL, A_PCL, D_PCL/PEO,* and *A_PCL/PEO.*

Samples	Peak designation	Band (eV)	At (%)	(O/C) ratio (%)
D_PCL	C 1s	285.07	68.8	36.1
	O 1s	532.07	24.8	
A_PCL	C 1s	284.98	70.6	34.7
	O 1s	532.48	24.5	
D_PCL/PEO	C 1s	284.97	63.5	50.2
	O 1s	531.47	31.9	
A_PCL/PEO	C 1s	285.98	66.4	45.2
	O 1s	532.48	30	

3.6. Surface morphology and wettability

The SEM micrographs of the surface morphology of the DIW printed samples are shown in Fig. 8 (a). The PCL surface printed from the DCM ink was smoother than that from the ACE ink; similarly, the printed PCL/PEO surface from the DCM ink had fewer wrinkles than the ACE system, indicating the influence of solvents on the surface morphology. The addition of PEO resulted in the introduction of bumps onto the filament surface (when compared with the PCL filaments). This happened in samples printed from both ACE- and DCM-based inks. The increase in the surface roughness of the printed PCL/PEO was further confirmed by surface roughness measurements. The arithmetic average roughness Ra obtained from a quantitative analysis of filaments on the top layers increased from 0.12 ± 0.01 μm to 0.28 ± 0.08 μm for the samples printed from the DCM-based inks; the roughness increased from 0.18 ± 0.02 μm to 0.49 ± 0.11 μm for the samples printed from the ACE-based inks.

The surface roughness (Ra) of printed samples from the ACE-based inks was significantly higher ($p < 0.05$) than those from the DCM ones, which indicates that the surface roughness of DIW-printed construct could be controlled by solvent selection. Tang *et al.* [44] showed that the surface of the solvent-casted PCL film using chloroform (a hydrophobic solvent) was smoother than that from ACE (a hydrophilic solvent), suggesting that the surface morphology could be dictated by the solubility of PCL in the respective solvent systems.

The contact angle (CA) is a measure of surface wettability [45]. The

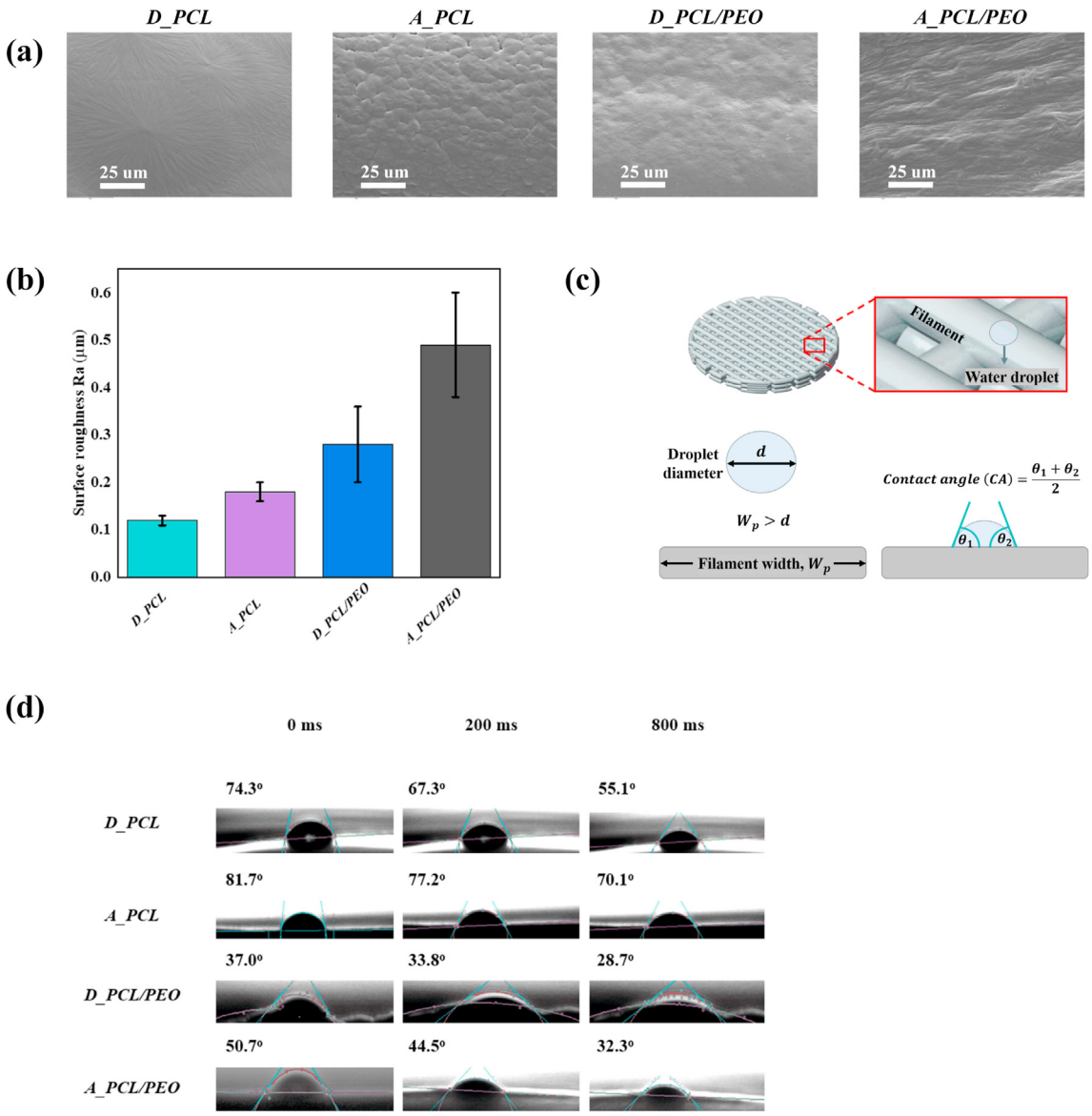

Fig. 8. SEM micrographs (a), surface roughness measurements (b), the schematic diagram of contact angle measurement (c), and water contact angle results at the time point of 0, 200 and 800 ms (d) on the filament surface of the printed samples - *D_PCL, A_PCL, D_PCL/PEO*, and *A_PCL/PEO*.

water contact angles on the filaments of the top layer of DIW printed samples are shown in Fig. 8 (c). The droplet volume used for the CA measurement was 4×10^{-4} μL; the diameter of the droplet was roughly 90 μm, which was smaller than the filament widths (ranging from 200 to 600 μm). Thus, it was possible to place the water droplets on top of a single filament. As shown in Fig. 8 (d), at the initial contact moment of a droplet on the printed filaments, the CAs were 74.3 ± 0.9°, 81.7 ± 4.0°, 37.0 ± 0.6° and 50.7 ± 0.3° for *D_PCL, A_PCL, D_PCL/PEO* and *A_PCL/PEO*, respectively (n = 3). As the time increased from 0 ms to 800 ms, the CA values for all samples gradually decreased. The CA values at 200 ms for sample *D_PCL*, *A_PCL*, *D_PCL/PEO*, and *A_PCL/PEO* were 67.3 ± 0.2°, 77.2 ± 0.2°, 33.8 ± 0.3° and 44.5 ± 0.3°. At 800 ms, the respective CA values were 55.1 ± 1.4°, 70.1 ± 0.5°, 28.7 ± 0.6° and 31.6 ± 0.7°. After 800 ms, the CA values become too small to be measured as the droplets were fully spread on the surfaces of PCL/PEO samples, which indicating that the filaments were wetted completely within less than 1 s.

The DCM-based inks resulted in smaller CA values on the printed samples than those made from ACE-based inks ($p < 0.05$); the incorporation of PEO reduced the CA values significantly ($P < 0.01$). The results suggest that both the type of solvent system and PEO addition had an impact on the wettability of DIW printed samples. This could be related to the higher O/C ratios measured from XPS. The samples made from the DCM-based inks had a greater O/C ratio than those from ACE-based inks; a further increase of 14% after the addition of PEO into PCL was noted. The results confirmed that the surface oxygen content is a good indicator of the wettability of the DIW-printed structure.

4. Discussion

In this study, both the type of solvent system and PEO incorporation in PCL ink had a noteworthy impact on the rheological performance. The initial viscosity (when shear rate equals 0.01 s^{-1}) of the ACE-based inks were generally greater than the DCM-based ones (with or without PEO incorporation). This may be resulted from the greater prevalence of interchain bonding in the ACE-water solvent system compared to the DCM system, which in turn leading to higher viscosity in the ACE-based inks at rest or low shear strains. Moreover, the values of the power law index *n* and the yield stress for all of the measurable ACE-based inks were smaller than the DCM-based inks. This result could be related to the difference in solvent polarity between the solvent systems as the blend of

ACE and water is more polar than DCM [46]; the interactions will differ both inter-molecularly (between the polymer chains) as well as between the solvent and solute molecules. In this context, the enhanced shear thinning exhibited by the ACE systems may reflect the greater propensity for temporary disruption of these interactions than is found for the DCM systems, for which there is a lower degree of initial internal bonding; in such systems, the application of stress will not result in the same decrease in viscosity. Although all the formulated inks presented in this study were shear-thinning non-Newtonian fluids, adequate recovery of viscosity (>80%) with the time-dependent increase was only achievable with PEO incorporation. This also implies that PCL-only inks would not be regarded as an ideal printable material. Therefore, this study demonstrates that incorporation of a polymer such as PEO can aid in processing of PCL by DIW printing.

The thermal results and XRD patterns shown in Fig. 7 confirmed the complete evaporation of solvents in the printed outcomes within 12 h, the improved thermal stability of PCL in the blended matrix and the immiscibility of PCL and PEO. The SEM and roughness results in our study corresponded to each other in that both indicated that the printed filaments made out of ACE based inks resulted in a rougher surface than DCM based ones; the addition of PEO further increased the micro-scale roughness. The results are understandable as both the type of solvent system and the incorporation of PEO would affect the proportion of the polymer-solvent and polymer-polymer interactions in the mixture, which ultimately regulates the entanglements among the polymer chains. It has been reported that a higher degree of polymer entanglements results in a more condensed and smoother surface after the solvent evaporation [30,44], which suggests that the entanglements are greater in the DCM-based solvent system than in the ACE-based solvent system and with the PEO incorporation. An interesting aspect of the roughness data is that the PCL filaments processed via DIW in this study were much rougher (Ra of 0.12 μm and 0.18 μm for filaments made from DCM-based and ACE-based inks, respectively) than those prepared using FDM (Ra of 0.02 μm) as reported by Jeon *et al.* [47]. This result could be attributed to the difference in the solidification between the two techniques. In FDM, the solidification occurs almost immediately after the melt; in DIW, the process depends on a slower solvent evaporation rate, which results in a rougher and uneven surface. Our results suggest that the surface morphology and roughness of a polymeric construct is tuneable when processed via DIW by varying the type of solvent system.

As stated earlier, the hydrophobic biomaterial PCL has been widely applied in tissue engineering field due to its ability to maintain integrity for tissue regeneration as well as facilitate long-term drug release profiles [8,9]. Dwivedi, Kumar *et al.* [48] indicate that these advantages are associated with PCL exhibiting a longer degradation time compared to other polyesters due to the presence of five hydrophobic –CH_2 moieties in the repeating unit [48]. However, studies also indicate that hydrophobic polymers such as PCL may hinder effective cell attachment and reduce cell affinity; as such, there may promote biological performance via improving the surface wettability [22,24,49].

In terms of the wettability results without PEO, the neat PCL filaments that were processed via DIW were more hydrophilic (initial CA of 74° and 82° on the filaments made out of DCM-based and ACE-based inks, respectively) than those prepared by other techniques. For instance, Wang *et al.* [50] prepared PCL scaffolds using FDM; the reported contact angle was 96.0° after 20s (using ~4 μL of water droplets on filaments that were 330 μm in diameter). Jeon *et al.* [47] also used FDM to print PCL scaffolds and placed a 10 μL droplet on the filaments with a diameter of 250 μm. The measured CA was 112.5° after 1s. Yew *et al.* [51] applied electrospinning to fabricate PCL nanofibers; the CAs were around 113° after 1 s using 10 μL of water droplets on PCL nanofibers. Furthermore, the CAs on PCL films that were produced via solvent casting ranged between 89.5° to 101.7° [44,52]. It is important to note that the volume of water droplets used in these studies and the data collection time points were not consistent, which may contribute towards the differences in measured CA. However, our CAs were measured based on the initial contact (the moment the droplet landed on the filaments); more importantly, the droplets wetted the surface of PCL filament completely within 1s. Hence, the printed PCL constructs have greater hydrophilicity than those made by other fabrication techniques, which could be related to the rougher surface obtained by DIW processing.

As shown from this study, DIW process has a tendency to produce PCL-based constructs with enhanced wettability and surface roughness. This finding could be particularly useful for biomedical applications as the hydrophobicity of PCL is often regarded as a performance weakness. Previous studies have attempted to apply treatments to the PCL surface [50] or create a blend with a hydrophilic material [25] as a way to improve cell growth and viability. Hence, the surface properties of the PCL-based matrix may be tuned with the aid of hydrophilic polymers such as PEO, thereby enhancing and expanding the usability of the material. In addition, the heat-free printing environment of DIW enables the incorporation of thermo-sensitive components in the ink formulation [15]. Therefore, the DIW process has the essential attributes to be a successful 3D fabrication tool in the biomedical field.

5. Conclusions

In this exploratory study, the PCL and PCL/PEO polymer inks have been formulated by dissolving PCL and PEO polymers into two solvent systems that are based on DCM and ACE. Upon increasing the concentration of PCL and PEO for both ACE and DCM inks, more marked shear-thinning behaviour has been observed. Although the ACE inks has more pronounced shear-thinning behaviour than the DCM inks, the viscosity recovery performance of the ACE-based inks is inferior to that of the DCM inks. Based on the mathematical modelling of the ink conditions within the nozzle under the same extrusion rate, the shear rate of the ACE-based ink is nine times higher than the DCM-based one; this parameter can be associated with the inconsistency of the printing process since there is insufficient recovery for the ACE-based inks over the process time window. We therefore suggest DCM over the ACE-based solvent system, particularly when using the PCL/PEO blend for the extrusion-based fabrication process.

Further, the DIW method has been applied to extrude the selected inks to fabricate woodpile structures in a layer-by-layer building sequence. The surface morphology, material characterisation, and wettability of the DIW printed PCL and PCL/PEO constructs are compared. The surface morphology results indicate that the ACE-based samples have a rougher surface than DCM-based ones; the addition of PEO further increases the microscale roughness. The wettability of DCM-based samples is higher than ACE-based ones; the wettability is further improved by blending PCL with PEO in both ACE- and DCM-based samples. Combining these outcomes, the DIW technique offers a new toolkit to develop a 3D construct with tuneable surface characteristics for biomedical applications.

Declaration of competing interest

The authors declare that they have no known competing financial interests or personal relationships that could have appeared to influence the work reported in this paper.

Acknowledgments

The financial support of China Scholarship Council (CSC) - UCL Joint research scholarship, and the Vest Scholarship of the US National Academy of Engineering (NAE) are gratefully acknowledged.

References

[1] H.H. Hwang, W. Zhu, G. Victorine, N. Lawrence, S. Chen, Small Methods 2 (2) (2018).
[2] R.L. Truby, J.A. Lewis, Nature 540 (7633) (2016) 371–378.

[3] R.J. Morrison, S.J. Hollister, M.F. Niedner, M.G. Mahani, A.H. Park, D.K. Mehta, R.G. Ohye, G.E. Green, Sci. Transl. Med. 7 (285) (2015), 285ra64.
[4] S.D. Gittard, R.J. Narayan, Expet Rev. Med. Dev. 7 (3) (2010) 343–356.
[5] D. Drummer, D. Rietzel, F. Kühnlein, Physics Procedia 5 (2010) 533–542.
[6] G.H. Wu, S.H. Hsu, Review: polymeric-based 3D printing for tissue engineering, J. Med. Biol. Eng. 35 (3) (2015) 285–292.
[7] J. Holländer, N. Genina, H. Jukarainen, M. Khajeheian, A. Rosling, E. Mäkilä, N. Sandler, J. Pharmaceut. Sci. 105 (9) (2016) 2665–2676.
[8] J.C. Reichert, M.E. Wullschleger, A. Cipitria, J. Lienau, T.K. Cheng, M.A. Schütz, G.N. Duda, U. Nöth, J. Eulert, D.W. Hutmacher, Int. Orthop. 35 (8) (2011) 1229–1236.
[9] Z. Zhou, Q. Yao, L. Li, X. Zhang, B. Wei, L. Yuan, L. Wang, Med. Sci. Mon. Int. Med. J. Exp. Clin. Res. 24 (2018) 6934.
[10] R. Song, M. Murphy, C. Li, K. Ting, C. Soo, Z. Zheng, Drug Des. Dev. Ther. 12 (2018) 3117.
[11] H.-J. Sung, C. Meredith, C. Johnson, Z.S. Galis, Biomaterials 25 (26) (2004) 5735–5742.
[12] E. Malikmammadov, T.E. Tanir, A. Kiziltay, V. Hasirci, N. Hasirci, Polymer edition 29 (7–9) (2018) 863–893.
[13] S.M. Espinoza, H.I. Patil, E. San Martin Martinez, R. Casañas Pimentel, P.P. Ige, International Journal of Polymeric Materials and Polymeric Biomaterials 69 (2) (2020) 85–126.
[14] P. Arunkumar, J.A. Dougherty, J. Weist, N. Kumar, M.G. Angelos, H.M. Powell, M. Khan, Nanomaterials 9 (7) (2019) 1037.
[15] J. Jang, J.Y. Park, G. Gao, D.W. Cho, Biomaterials 156 (2018) 88–106.
[16] J.A. Lewis, G.M. Gratson, Mater. Today 7 (7) (2004) 32–39.
[17] J.L. Dávila, M.A. d'Ávila, Int. J. Adv. Manuf. Technol. 101 (1–4) (2019) 675–686.
[18] R.A. Barry III, R.F. Shepherd, J.N. Hanson, R.G. Nuzzo, P. Wiltzius, J.A. Lewis, Adv. Mater. 21 (23) (2009) 2407–2410.
[19] B. Zhang, R. Cristescu, D. Chrisey, R. Narayan, International Journal of Bioprinting 6 (2020) 19.
[20] J. Malda, J. Visser, F.P. Melchels, T. Jungst, W.E. Hennink, W.J. Dhert, J. Groll, D.W. Hutmacher, Adv. Mater. 25 (36) (2013) 5011–5028.
[21] Y. He, F. Yang, H. Zhao, Q. Gao, B. Xia, J. Fu, Sci. Rep. 6 (2016) 29977.
[22] M.G. Yeo, G.H. Kim, Chem. Mater. 24 (5) (2012) 903–913.
[23] Y. Li, Z.-g. Wu, X.-k. Li, Z. Guo, S.-h. Wu, Y.-q. Zhang, L. Shi, S.-h. Teoh, Y.-c. Liu, Z.-y. Zhang, Biomaterials 35 (22) (2014) 5647–5659.
[24] L. Dong, S.-J. Wang, X.-R. Zhao, Y.-F. Zhu, J.-K. Yu, Sci. Rep. 7 (1) (2017) 1–9.
[25] K.R. Remya, S. Chandran, S. Mani, A. John, P. Ramesh, J. Biomater. Sci. Polym. Ed. 29 (12) (2018) 1444–1462.
[26] Z. Qiu, T. Ikehara, T. Nishi, Polymer 44 (10) (2003) 3101–3106.
[27] B. Dorj, J.E. Won, J.H. Kim, S.J. Choi, U.S. Shin, H.W. Kim, J. Biomed. Mater. Res. 101 (6) (2013) 1670–1681.
[28] E.M. Goncalves, F.J. Oliveira, R.F. Silva, M.A. Neto, M.H. Fernandes, M. Amaral, M. Vallet-Regi, M. Vila, J. Biomed. Mater. Res. B Appl. Biomater. 104 (6) (2016) 1210–1219.
[29] H. Maleki, A.A. Gharehaghaji, L. Moroni, P.J. Dijkstra, Biofabrication 5 (3) (2013), 035014.
[30] A. Entezari, Z. Zhang, A. Sue, G. Sun, X. Huo, C.-C. Chang, S. Zhou, M.V. Swain, Q. Li, Journal of the mechanical behavior of biomedical materials 89 (2019) 150–161.
[31] S. Shenoy, W. Bates, H. Frisch, G. Wnek, Polymer 46 (2005) 3372–3384.
[32] F. Morrison, Understanding Rheology, Oxford University Press, New York, 2001.
[33] C.W. Macosko, R.G. Larson, Rheology: Principles, Measurements, and Applications, 1994.
[34] N. Paxton, W. Smolan, T. Böck, F. Melchels, J. Groll, T. Jungst, Biofabrication 9 (4) (2017), 044107.
[35] G.S. Blair, J. Hening, A. Wagstaff, J. Phys. Chem. 43 (7) (1939) 853–864.
[36] C.W. Peak, J. Stein, K.A. Gold, A.K. Gaharwar, Langmuir 34 (3) (2018) 917–925.
[37] D.X. Chen, D.X. Chen, Glaser, Springer, 2019.
[38] B. Zhang, R. Cristescu, D.B. Chrisey, R.J. Narayan, Solvent-based Extrusion 3D Printing for the Fabrication of Tissue Engineering Scaffolds.
[39] A. Bruyas, F. Lou, A.M. Stahl, M. Gardner, W. Maloney, S. Goodman, Y.P. Yang, J. Mater. Res. 33 (14) (2018) 1948–1959.
[40] B. Dillon, P. Doran, E. Fuenmayor, A.V. Healy, N.M. Gately, I. Major, J.G. Lyons, Polymers 11 (4) (2019) 710.
[41] E. Abdelrazek, A. Hezma, A. El-Khodary, A. Elzayat, Egyptian Journal of Basic and Applied Sciences 3 (1) (2016) 10–15.
[42] N.M. Nasir, N.M. Zain, M. Raha, N. Kadri, Am. J. Appl. Sci. 2 (12) (2005) 1578–1583.
[43] G. Zhou, C. Xu, W. Cheng, Q. Zhang, W. Nie, Journal of analytical methods in chemistry (2015), 467242, 2015.
[44] Z. Tang, R. Black, J. Curran, J. Hunt, N. Rhodes, D. Williams, Biomaterials 25 (19) (2004) 4741–4748.
[45] P. Dubey, B. Bhushan, A. Sachdev, I. Matai, S. Uday Kumar, P. Gopinath, J. Appl. Polym. Sci. 132 (35) (2015).
[46] C.M. Hansen, CRC press, 2007.
[47] H. Jeon, H. Lee, G. Kim, Tissue Eng. C Methods 20 (12) (2014) 951–963.
[48] R. Dwivedi, S. Kumar, R. Pandey, A. Mahajan, D. Nandana, D.S. Katti, D. Mehrotra, Journal of Oral Biology and Craniofacial Research 10 (1) (2020) 381–388.
[49] N. Siddiqui, S. Asawa, B. Birru, R. Baadhe, S. Rao, Mol. Biotechnol. 60 (7) (2018) 506–532.
[50] W. Wang, G. Caetano, W.S. Ambler, J.J. Blaker, M.A. Frade, P. Mandal, C. Diver, P. Bártolo, Materials 9 (12) (2016) 992.
[51] C.H.T. Yew, P. Azari, J.R. Choi, F. Muhamad, B. Pingguan-Murphy, Polymers 10 (12) (2018) 1387.
[52] D.S. Jones, J. Djokic, C.P. McCoy, S.P. Gorman, Biomaterials 23 (23) (2002) 4449–4458.